10.1109/ULTSYM.2015.0378

Shear Wave Estimation using Null Space Pursuit and AM-FM Demodulation

Renán Rojas*, Juvenal Ormachea†, Kevin J. Parker†, Benjamin Castaneda*
*Departamento de Ingeniería, Sección Electricidad y Electrónica
Pontificia Universidad Católica del Perú, Lima, Peru
†Department of Electrical & Computer Engineering
University of Rochester, Rochester, New York, USA

***Abstract*—Crawling wave sonoelastography enables the measurement of viscoelastic properties of soft tissue. Recently, the dominant component analysis AM-FM method was proposed for modeling non-stationary patterns in crawling wave sonoelastography to locally estimate their shear wave speed. Although evaluations show consistent results for homogeneous and inhomogeneous phantoms, high noise levels and few available data samples do not allow a rigorous spectral analysis by using a filterbank. We propose a novel method to isolate AM-FM components based on the null space pursuit algorithm that alleviates such limitations. Preliminary results for the proposed method for homogeneous and inhomogeneous phantoms, and a comparison to alternative methods are presented.**

I. Introduction

Crawling wave sonoelastography is a method for quantifying tissue elasticity whereby shear wave speed is visualized in the interference patterns of two sources oscillating at slightly different frequencies [1]. Since its introduction, many data processing approaches have been proposed, enabling its application to different types of human tissue [2], [3], [4], [5].

Recently, an information extraction approach proposed the use of the Amplitude Modulation - Frequency Modulation model (AM-FM) [6], [7] to characterize the interference pattern as a sum of quasisinusoidal components with instantaneous amplitude and frequency modulation functions. The proposed shear wave speed estimation method [8] was based on the Dominant Component Analysis paradigm (DCA) [9], which employs conjointly spatio-spectrally localized filters to isolate the strongest component and then demodulate it using the quasi-eigenfunction approximation (QEA) [10] to compute the local shear wave speed.

Despite promising results, evaluations showed that the AM-FM subcomponent isolation using a filterbank has considerable limitations when applied to crawling wave data. The interference pattern is characterized as a narrowband signal with a low frequency range, which requires highly spectrally localized filters to isolate it. Also, its local nonstationarities must be represented by the few available samples in the space domain, which cover a limited number of interference pattern periods. These conditions do not permit the proper use of conjointly spatio-spectrally localized filters capable of reducing cross-channel interferences and subsequent demodulation errors.

Among the alternatives for signal separation tasks, null space pursuit is an approach that "annihilates" a signal subcomponent included in the null space of an adaptive differential operator by solving a convex optimization problem. This algorithm has been successfully used to isolate narrowband subcomponents by an iterative single-channel approach [11].

The present work proposes a method for estimating the local shear wave speed using the AM-FM model and the null space pursuit algorithm as an alternative to the filterbank approach. Furthermore, a denoising stage based on a low-rank approximation is proposed prior to the demodulation task to reject spurious components that may affect the estimation accuracy. Then, the local shear wave speed is estimated by the local oscillation rate across the tissue. The rest of the document is organized as follows: Section II introduces the theoretical definitions required for establishing the framework of interest, Section III presents the proposed method, Section IV contains the experimental results, and finally Section V presents the conclusions and further work details.

II. Theoretical Background

A. Crawling Waves Sonoelastography

Under a plane wave assumption, the shear waves introduced by two opposite external vibration sources oscillating with slightly different frequencies form an interference pattern with squared signal envelope $|u(x,t)|^2$ modeled by:

$$|u(x,t)|^2 = 2e^{-\alpha D}\{\cosh(2\alpha x) + \cos[(2k+\Delta k)x + \Delta\omega t]\}; \quad (1)$$

where D is the distance between oscilation sources, α is the attenuation factor, k is the local shear wave spatial frequency and $\Delta\omega$ is the frequency difference between the vibration sources [1]. Focusing on the central region of the material and assuming weak wave attenuations, the hyperbolic cosine becomes constant and (1) approximated by [5]

$$|u(x,t)|^2 \approx 2e^{-\alpha D}\cos[(2k+\Delta k)x + \Delta\omega t]. \quad (2)$$

The shear wave speed V_{shear} and the elasticity modulus E are then defined as $V_{\text{shear}} = f \cdot k^{-1}$ and $E = 3\rho V_{\text{shear}}^2$, where f is the operating frequency in Hz and ρ the mass density of the material.

978-1-4799-8182-3/15/$31.00 ©2015 IEEE

B. Amplitude Modulation - Frequency Modulation Model

The AM-FM model represents an oscillatory signal as a sum of elements expressed as $t(\mathbf{x}) = \sum_{i=0}^{N-1} a_i(\mathbf{x}) e^{j\varphi_i(\mathbf{x})}$, where each component $t_i(\mathbf{x}) = a_i(\mathbf{x}) e^{j\varphi_i(\mathbf{x})}$ is a complex-valued narrowband signal formed by an instantaneous amplitude (IA) function a_i, an instantaneous phase (IP) function φ_i, and an instantaneous frequency (IF) function $\nabla\varphi_i$.

Given a real-valued multi-component signal $r(\mathbf{x}) = \sum_{i=0}^{N-1} a_i(\mathbf{x}) \cos[\varphi_i(\mathbf{x})]$, its complex extension $t(\mathbf{x})$ is derived by establishing a unique imaginary part based on the Hilbert transform $\mathcal{H}$ as $t(\mathbf{x}) = r(\mathbf{x}) + j\mathcal{H}\{r(\mathbf{x})\}$. Then, the signal local properties may be described by the DCA multi-component paradigm, which models the signal non-stationary behavior at each $\mathbf{x}$ coordinate by exclusively taking into account the AM-FM component with the strongest response [12].

Finally, the corresponding IF and IA functions can be accurately estimated with support in the four quadrants by the discrete QEA algorithm [9].

C. Operator-based Signal Separation: Null Space Pursuit

Null space pursuit (NSP) is a signal separation algorithm that isolates narrowband elements from a multi-component input signal using the null space of a differential operator. This operator is derived from the input signal and its model depends on the properties of the narrowband signal of interest. NSP has been successfully used to separate a set of narrowband subcomponents by an iterative single-channel approach [13].

The method is established as a convex minimization problem that isolates subcomponent V from the multi-component signal S. This minimization problem computes the residual signal R such that $S = V + R$ in the following way:

$$\underset{R}{\operatorname{argmin}} ||\mathcal{T}_{\mathcal{S}}(S-R)||_2^2 + \lambda\big(||D(R)||_2^2 + \gamma||S-R||_2^2\big) + \mathcal{F}(\mathcal{T}_{\mathcal{S}}); \tag{3}$$

where $\mathcal{T}_{\mathcal{S}}$ is the adaptive differential operator established based on the properties of the subcomponent V, i.e. $(S-R)$ is in the null space of the operator $\mathcal{T}_{\mathcal{S}}$, and D is the differential operator. The scalar γ defines the amount of information from subcomponent V retained in the null space of $\mathcal{T}_{\mathcal{S}}$, and $\mathcal{F}(\mathcal{T}_{\mathcal{S}})$ corresponds to the Lagrange term for $\mathcal{T}_{\mathcal{S}}$ [11].

A set of subcomponents can be isolated in an iterative approach by "annihilating" them from subsequent residual signals, leading to a multi-component separation approach. Assuming a 1D real-valued signal composed of a sum of AM-FM components $s(t) = \sum_{i=0}^{N-1} a_i(t)\cos(\varphi_i(t))$, a second-order differential null space operator is proposed for AM-FM subcomponents as [14]: $\mathcal{T}_{\mathcal{S}} = \frac{d^2}{dt^2} + P(t)\frac{d}{dt} + Q(t)$. Thus, each component is isolated by the NSP approach by estimating $P(t)$ and $Q(t)$ such that $\mathcal{T}_{\mathcal{S}} \cdot [a(t)\cos(\varphi(t))] = 0$. Then, the NSP approach for isolating AM-FM subcomponents becomes:

$$\begin{aligned}\underset{P,Q,R}{\operatorname{argmin}} ||\mathcal{T}_{\mathcal{S}}(S-R)||_2^2 + \lambda_1\Big(||R||_2^2 + \gamma||S-R||_2^2\Big) \\ +\lambda_2\Big(||D_2(Q)||_2^2 + ||P||_2^2\Big).\end{aligned} \tag{4}$$

III. Proposed Method

A. Pre-processing Approach

An average filter is used along the lateral dimension vs. frames plane to preserve only the non-stationary term. Then, the slow-time signal behavior is used to remove noise by applying a linear-phase bandpass filter centered at $\Delta\omega$.

Since the interference pattern varies exclusively along the lateral dimension and along frames, changes along the axial dimension depend only on the appearance of a material with different elasticity modulus. Thus, its changes are structured and coherent rather than abrupt. By taking advantage of this, we propose to further remove distortions by computing a low-rank approximation. An alternative representation of the ultrasound data is obtained by vectorizing each lateral dimension vs. frames plane and building a column-wise 2D representation of the ultrasound data. Given the ultrasound volume $f \in \mathbb{R}^{M\times N\times T}$, the vectorized version of each spatio-temporal plane $\bar{f}_{y_i} = \text{vec}\{f(y_i, x, t)\}$ is computed. Then, the matrix $F \in \mathbb{R}^{NT\times M}$ is defined as $F = [\bar{f}_{y_0}, \bar{f}_{y_1}, \ldots, \bar{f}_{y_{M-1}}]$.

The low-rank approximation of matrix F is then computed by using a fixed number of its largest eigenvalues. The low-rank approximation process is performed by a singular value decomposition routine. Finally, the information comprised in the low-rank output is reverted to its original dimensions.

B. Signal Isolation and Demodulation Stage

The NSP algorithm is employed to isolate the narrowband subcomponent with the highest energy. For this purpose, a fixed number of narrowband signals are isolated and the one with the highest ℓ^2 norm is preserved. Then, its 1D instantaneous frequency along the lateral dimension is estimated via the QEA method for each frame. Finally, the effective instantaneous frequency at each point along the lateral dimension is established as the median of its instantaneous frequency estimations across frames.

IV. Experimental Results

A. Pre-processing Approach Performance

Inhomogeneous phantom simulations corrupted by speckle noise are processed using the low-rank approach. The noise model is defined as $b(\mathbf{x}) = f(\mathbf{x}) + \mathcal{U}\cdot f(\mathbf{x})$, where $\mathcal{U}$ is uniformly distributed with zero mean and variance σ^2 ranging from 0.1 to 1 in steps of 0.1. In all cases, the ground truth local velocities are 8 m/s for the inclusion and 4 m/s for the background. Table I shows the signal to noise ratio (SNR) between the noise-corrupted phantoms and their corresponding noise-free versions. Table II shows the SNR between low-rank approximations for different rank values and their corresponding noise-free versions, showing a considerable similarity improvement with its largest values at rank 5 in most cases. Figure 1 describes a portion of matrix F for the $\sigma^2 = 0.5$ speckle noise corrupted simulation and its low-rank approximation for a fixed rank value of 5. It can be observed that the inclusion is modeled as a pattern with low frequency along rows located in the central region.

TABLE I

SNR (DB) BETWEEN THE NOISE-FREE DATA AND THE NOISE-CORRUPTED DATA.

σ^2	0.1	0.2	0.3	0.4	0.5	0.6	0.7	0.8	0.9	1
	4.6	3.7	3.1	2.6	2.2	2.0	1.8	1.7	1.6	1.5

TABLE II

SNR (DB) BETWEEN THE NOISE-FREE DATA AND THE LOW-RANK OUTPUT.

σ^2 | rank	3	5	7	9	11	13	15
0.1	18.0	**18.6**	18.6	18.6	18.5	18.5	18.5
0.2	14.7	**14.9**	14.9	14.9	14.9	14.9	14.9
0.3	12.8	**12.9**	12.9	12.9	12.8	12.8	12.8
0.4	11.4	**11.5**	11.5	11.5	11.5	11.5	11.5
0.5	10.6	**10.7**	10.7	10.6	10.6	10.6	10.6
0.6	9.9	**10.0**	10.0	10.0	10.0	9.9	9.9
0.7	9.5	**9.6**	9.5	9.5	9.5	9.5	9.5
0.8	9.2	**9.3**	9.2	9.1	9.1	9.1	9.1
0.9	8.9	**9.0**	8.9	8.8	8.8	8.8	8.8
1	**8.7**	8.6	8.6	8.6	8.6	8.6	8.5

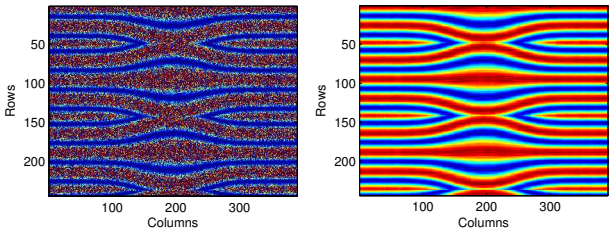

(a) (b)

Fig. 1. F matrix portion for an inhomogeneous phantom: (a) F for the noisy data. (b) F after the low-rank approximation.

The low-rank approximation removes the large changes while preserving the low variabilities of the interference pattern.

B. Speed Estimation Performance on Simulated Phantoms

Figure 2 shows the signal isolation process using the NSP algorithm along an inhomogeneous region. Although the low-rank approximation results in a consistent reconstruction, several subcomponents are still included. However, the NSP method recovers with high accuracy the non-stationary signal, which is subsequently demodulated. Figure 3 shows shear wave speed (SWS) maps for inhomogeneous phantoms with $\sigma^2 = 0.1$ and $\sigma^2 = 0.7$ speckle noise. The real inclusion regions are denoted by a blue circle. Although the noise level has a strong effect in the inclusion location and contrast, overall it is accurately located, no considerable artifacts are created, and the speed estimations are highly accurate.

C. Speed Estimation Performance on Gelatin Phantoms

The proposed method is evaluated on gelatin phantoms at frequencies ranging from 140 Hz to 360 Hz in steps of 20 Hz. For the homogeneous case, the mean speed and standard deviation are computed at each frequency and compared with mechanical measurements obtained by stress relaxation tests. The relaxation curve is then fit to the Kelvin-Voigt Fractional

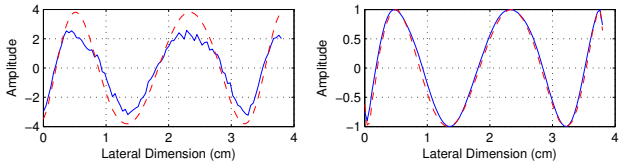

(a) (b)

Fig. 2. Pre-processing on an inclusion region: (a) Low-rank output (red) vs. noise-free data (blue). (b) Normalized NSP output (red) vs. normalized noise-free data (blue).

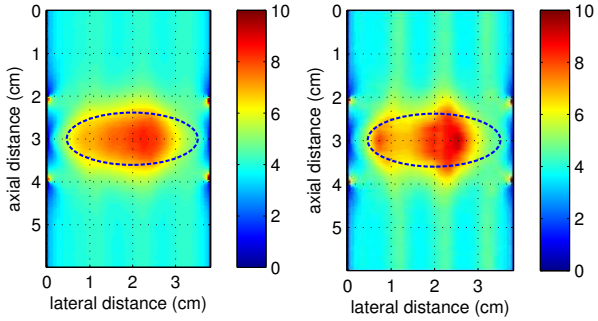

(a) (b)

Fig. 3. SWS maps of crawling waves data simulations with a large inclusion. (a) $\sigma^2 = 0.1$ speckle noise. (b) $\sigma^2 = 0.7$ speckle noise.

Derivative. Table III describes the phantom set composition. The equipment used in the experiments is listed in [8].

Figure 4 shows the estimated shear wave average speed and standard deviation for an homogeneous 10% gelatin phantom. Overall, speed estimations below 220 Hz show large deviations, indicating that lower spatial frequencies and fewer interference pattern periods decrease the estimation accuracy. For high operating frecuencies, variability consistently decreases.

Figure 5 compares the SWS maps of a 0.68 cm radius inclusion phantom for the proposed method (NSP AM-FM) and two alternative methods: phase derivation (CWS PD) [15] and the dominant component analysis (DCA AM-FM) [8]. Although the three approaches generate artifacts near the inclusion, the CWS PD results contains the largest ones. The DCA AM-FM results show less artifacts but its inclusion region shortens and its contrast gets penalized. The NSP AM-FM results show less artifacts than the CWS PD method, while accurately locating the inclusion region and increasing its contrast in comparison to the DCA AM-FM method.

V. CONCLUSIONS

A novel method for estimating the local shear wave speed using crawling waves is proposed based on the AM-FM model and the NSP algorithm. Its main contribution is the narrowbank signal isolation process, which does not require a filterbank to preserve the dominant non-stationary signal from ultrasound data. Furthermore, its main difference from previous methods is the use of the entire ultrasound volume to reject signal distortions while preserving the coherence of the interference pattern behavior using a low-rank approximation.

TABLE III
PHANTOM SET COMPOSITION.* GELATIN: 300 BLOOM TYPE A PORK 40 MESH.** GRAPHITE: POWDER G67-500.

	Inhomogeneous		**Homogeneous**
	Inclusion	*Background*	*10% Gelatin*
Degassed water (ml)	150	1800	1800
NaCl (g)	1.35	16.2	16.2
Gelatin* (g)	28.57	200	200
Graphite** (g)	18	36	36

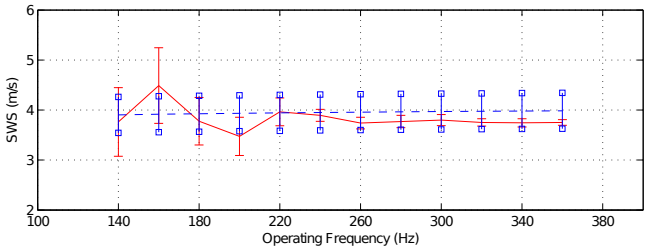

(a)

Fig. 4. SWS maps for an homogeneous 10% gelatin phantom: Proposed method (red) vs. mechanical measurements (blue).

Experimental results for the pre-processing approach show accuracy of volume restoration on artificial phantoms with different noise levels. Additionally, speed estimations for homogeneous phantoms show that there is still a large variation at low operating frequencies, while greater accuracy is achieved at high operating frequencies. Finally, experimental results for inhomogeneous phantoms shows an accurate inclusion location, a contrast improvement, and a reduction in the artifacts compared with the phase derivation method and the dominant component analysis AM-FM method.

Further research will focus on the use of principal component pursuit to establish the optimal rank value, a more robust null space operator to increase the signal isolation performance, and a 2D instantaneous frequency demodulation method to improve the speed estimation accuracy.

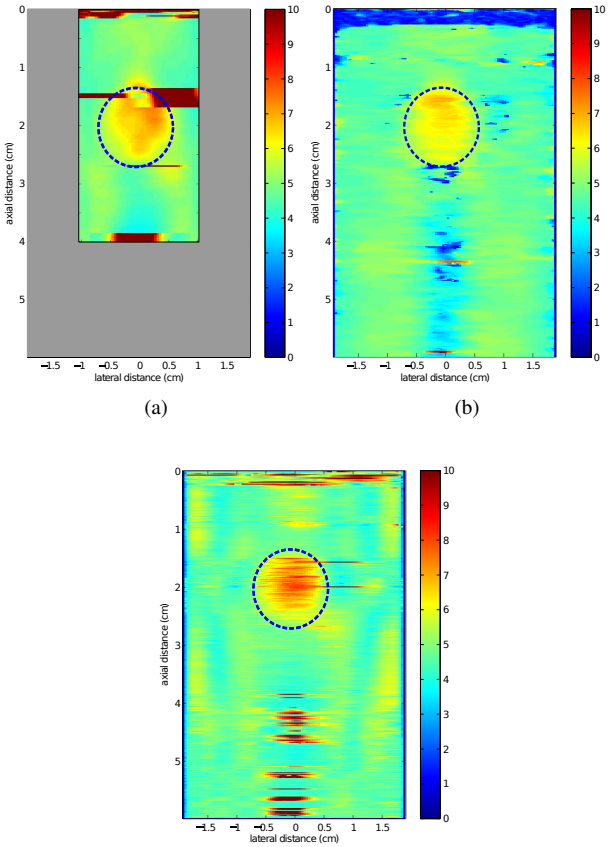

(a) (b)

(c)

Fig. 5. SWS maps for an inhomogeneous gelatin phantom. (a) CWS PD. (b) DCA AM-FM. (c) NSP AM-FM.

REFERENCES

[1] Z. Wu, L. S. Taylor, D. J. Rubens, and K. J. Parker, "Sonoelastographic imaging of interference patterns for estimation of the shear velocity of homogeneous biomaterials," *Physics in medicine and biology*, vol. 49, no. 6, p. 911, 2004.

[2] K. Hoyt, B. Castaneda, and K. J. Parker, "Two-dimensional sonoelastographic shear velocity imaging," *Ultrasound in medicine & biology*, vol. 34, no. 2, pp. 276–288, 2008.

[3] M. Zhang, B. Castaneda, Z. Wu, P. Nigwekar, J. V. Joseph, D. J. Rubens, and K. J. Parker, "Congruence of imaging estimators and mechanical measurements of viscoelastic properties of soft tissues," *Ultrasound in medicine & biology*, vol. 33, no. 10, pp. 1617–1631, 2007.

[4] K. Hoyt, T. Kneezel, B. Castaneda, and K. J. Parker, "Quantitative sonoelastography for the in vivo assessment of skeletal muscle viscoelasticity," *Physics in medicine and biology*, vol. 53, no. 15, p. 4063, 2008.

[5] B. Castaneda, "Extracting Information from Sonoelastographic Images," Ph.D. dissertation, University of Rochester, 2009.

[6] P. Maragos and A. C. Bovik, "Image demodulation using multidimensional energy separation," *JOSA A*, vol. 12, no. 9, pp. 1867–1876, 1995.

[7] J. P. Havlicek, D. S. Harding, and A. C. Bovik, "Reconstruction from the multi-component AM-FM image representation," in *Image Processing, 1995. Proceedings., International Conference on*, vol. 2. IEEE, 1995, pp. 280–283.

[8] R. Rojas, J. Ormachea, A. Salo, P. Rodríguez, K. J. Parker, and B. Castaneda, "Crawling Waves Speed Estimation Based on the Dominant Component Analysis Paradigm," *Ultrasonic imaging*, p. 0161734614568651, 2015.

[9] J. P. Havlicek, "AM-FM image models," Ph.D. dissertation, University of Texas at Austin, 1996.

[10] J. P. Havlicek, D. S. Harding, and A. C. Bovik, "Discrete quasi-eigenfunction approximation for am-fm image analysis," in *Image Processing, 1996. Proceedings., International Conference on*, vol. 1. IEEE, 1996, pp. 633–636.

[11] S. Peng and W.-L. Hwang, "Null space pursuit: An operator-based approach to adaptive signal separation," *Signal Processing, IEEE Transactions on*, vol. 58, no. 5, pp. 2475–2483, 2010.

[12] J. P. Havlicek, D. S. Harding, and A. C. Bovik, "Multidimensional quasi-eigenfunction approximations and multicomponent AM-FM models," *Image Processing, IEEE Transactions on*, vol. 9, no. 2, pp. 227–242, 2000.

[13] X. Hu, S. Peng, and W.-L. Hwang, "Estimation of instantaneous frequency parameters of the operator-based signal separation method," *Advances in Adaptive Data Analysis*, vol. 1, no. 04, pp. 573–586, 2009.

[14] X. Hu, S. Peng, and W.-L. Hwang, "Multicomponent AM-FM signal separation and demodulation with null space pursuit," *Signal, Image and Video Processing*, vol. 7, no. 6, pp. 1093–1102, 2013.

[15] J. Ormachea, R. Rojas, P. Rodriguez, R. J. Lavarello, K. J. Parker, and B. Castaneda, "Shear Wave Speed Estimation from Crawling Wave Sonoelastography: A comparison between AM-FM Dominant Component Analysis and Phase Derivation Methods," in *Ultrasonics Symposium (IUS), 2014 IEEE International*. IEEE, 2014, pp. 2327–2330.